Quantitative Analysis of the Water Occupancy around the Selectivity Filter of a K⁺ Channel in Different Gating Modes

Markus Weingarth,*,[†] Elwin A. W. van der Cruijsen,[†] Jared Ostmeyer,[‡] Sylke Lievestro,[†] Benoît Roux,[‡] and Marc Baldus*,[†]

[†]NMR Spectroscopy, Bijvoet Center for Biomolecular Research, Department of Chemistry, Faculty of Science, Utrecht University, 3584 CH Utrecht, The Netherlands

[‡]Department of Biochemistry and Molecular Biology, The University of Chicago, 929 E57th Street Chicago, Illinois 60637, United States

Ⓢ Supporting Information

ABSTRACT: Recovery in K⁺ channels, that is, the transition from the inactivated nonconductive selectivity filter conformation toward the conductive conformation, occurs on a time scale of the order of seconds, which is astonishingly long, given that the structural differences among the filter conformations are faint (<1 Å). Computational studies and electrophysiological measurements suggested that buried water molecules bound behind the selectivity filter are at the origin of the slowness of recovery in K⁺ channels. Using a combination of solid-state NMR spectroscopy (ssNMR) and long molecular dynamics simulations, we sketch a high-resolution map of the spatial and temporal distribution of water behind the selectivity filter of a membrane-embedded K⁺ channel in two different gating modes. Our study demonstrates that buried water molecules with long residence times are spread all along the rear of the inactivated filter, which explains the recovery kinetics. In contrast, the same region of the structure appears to be dewetted when the selectivity filter is in the conductive state. Using proton-detected ssNMR on fully protonated channels, we demonstrate the presence of a pathway that allows for the interchange of buried and bulk water, as required for a functional influence of buried water on recovery and slow inactivation. Furthermore, we provide direct experimental evidence for the presence of additional ordered water molecules that surround the filter and that are modulated by the channel's gating mode.
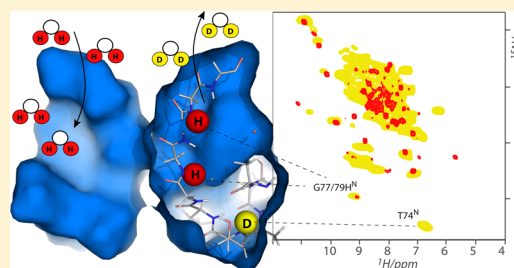
■ INTRODUCTION

Potassium (K⁺) channels share a common pore architecture for catalyzing the diffusion of ions across membranes.[1,2] Ion passage is controlled by two coupled gates.[3−6] They are located at either end of the channel pore and called the activation and inactivation gates. The inactivation gate is also known as the selectivity filter. Activation gating is associated with relatively large hinge-bending and rotational motions of the inner helix bundle, dilating the pore by about one nanometer upon channel opening.[7] In contrast, inactivation gating is accompanied by angstrom-scale local structural changes within the selectivity filter.[8−12] Crystal structures of KcsA from *Streptomyces lividans* obtained at low (3 mM, PDB: 1K4D) and high (200 mM, PDB: 1K4C) K⁺ concentration [K⁺][13] are commonly considered as representative for the closed-inactivated and closed-conductive channel gating modes, respectively.[8,14] According to these conformations, rearrangements within the selectivity filter upon inactivation are confined to a partial flip of the V76−G77 peptide plane, pinching the filter shut. The small structural differences between the conductive and inactivated selectivity filter, however, stand in sharp contrast to the remarkably long time scale of seconds on which recovery from slow inactivation, that is, transition from the inactivated toward the conductive filter state, occurs. Recent

molecular dynamics (MD) simulations[15] showed that this apparent discrepancy could be explained by the dynamics of buried water molecules bound in the back of the inactivated selectivity filter, which lock the filter in the inactivated state. MD simulations further predicted that conversion to a dewetted conductive state could only occur upon release of the inactivating water to the bulk, which was indirectly corroborated by the measurement of an accelerated recovery rate at high osmotic stress.

In a broader sense, such buried water molecules can be considered as an inherent part of the channel structure. Nevertheless, many unanswered questions remain regarding the mechanism by which the water modulates the free energy landscape associated with the conformational space of the selectivity filter, and how the distinct water occupancies are correlated with different filter conformations.[16] Previously, we have demonstrated that solid-state nuclear magnetic resonance (ssNMR) is a powerful technique to study the structural and dynamical properties of membrane-embedded KcsA variants before and after channel inactivation.[6,9,12] Here, we combined ssNMR studies with long MD simulations to provide a high-
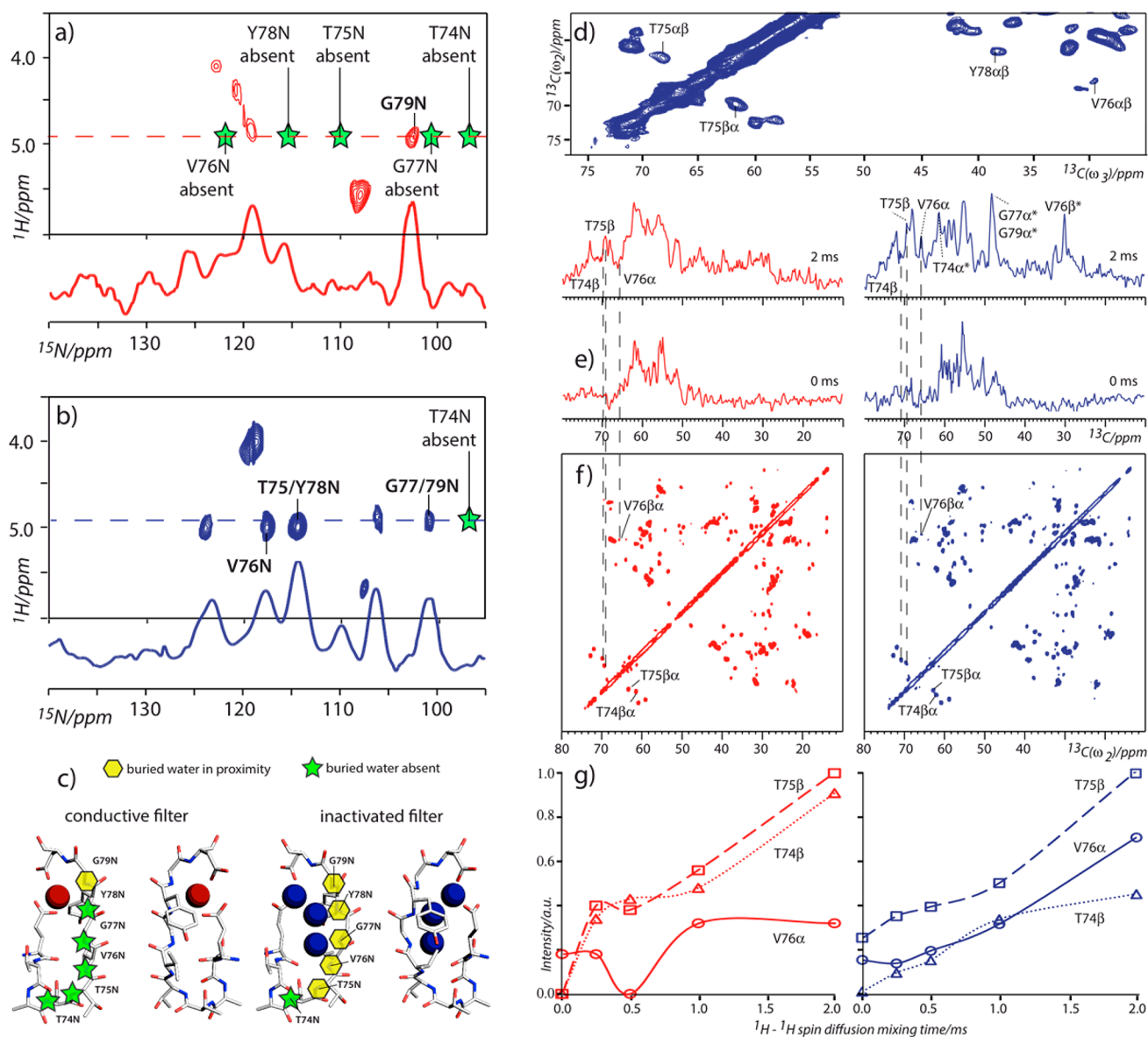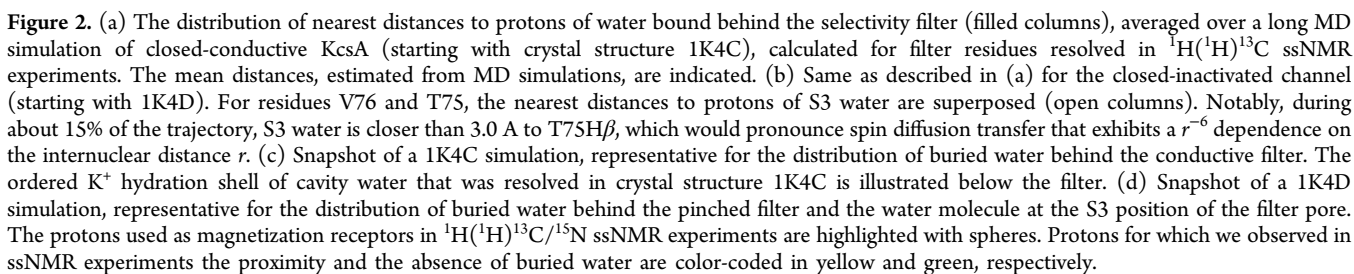
Figure 1. 2D ^{1}H(^{1}H)^{15}N ssNMR spectra of membrane-embedded KcsA in (a) the closed-conductive and (b) the open-inactivated state, measured at 52 kHz MAS. Cross sections along ω_2 at the ^{1}H water resonance are shown for both channel states. (c) The spatial distribution and content of crystal water behind the conductive (left, PDB: 1K4C) and inactivated (right, PDB: 1K4D) selectivity filter are consistent with our ^{1}H(^{1}H)^{15}N ssNMR data. Yellow hexagons and green stars indicate ^{15}N nuclei for which ssNMR experiments suggest the presence and the absence of buried, nearby water molecules, respectively. (d) ^{13}C−^{13}C plane at the ^{1}H water resonance of a 3D ^{1}H(^{1}H)^{13}C^{13}C spectrum measured on open-inactivated KcsA. (e) Cross sections, extracted from a series of 2D ^{1}H(^{1}H)^{13}C measurements with varying ^{1}H spin diffusion time (2 and 0 ms from top to bottom), along ω_2 at the water resonances for both the conductive (red, left panel) and the inactivated (blue, right panel) state. Signals that are ambiguous due to spectral overlap are marked with asterisks. (f) T74, T75, and V76 resonances can be retraced in PARIS[17,18] ^{13}C−^{13}C spin diffusion spectra for conductive (red, left) and inactivated filter (blue, right) conformation. (g) Build-up curves at the ^{1}H water resonance in the conductive (red, left) and inactivated (blue, right) conformations, extracted from a series of 2D ^{1}H(^{1}H)^{13}C experiments. Signal intensities were deduced from peak heights (T74C$_\beta$ in dotted lines and triangles, T75C$_\beta$ in dashed lines and squares, and V76C$_\alpha$ in continuous lines and circles). For each panel, the plots were normalized with respect to the most intense cross peak.

resolution spatial and temporal arrangement of buried water in the rear of the conductive and the inactivated filter of membrane-embedded KcsA, which corroborates that buried water is at the molecular origin of the slowness of recovery. Moreover, we demonstrate the use of high-resolution ^{1}H detected ssNMR on a fully protonated membrane protein to dissect in atomic detail a pathway that allows the interchange of buried and bulk water, as it was suggested to be required for recovery and slow inactivation. Finally, we provide direct experimental evidence for the presence of other sources of

ordered water that surround the filter and that are modulated by the states of the activation and inactivation gates.

■ RESULTS AND DISCUSSION

Spatial Distribution of Ordered Water around the Selectivity Filter before and after Inactivation. In general, ssNMR experiments can report on water proximities by making use of the distinct ^{1}H chemical shift of the water resonance and the fact that polarization transfer schemes such as cross-polarization (CP) or longitudinal mixing report, in the initial

Figure 2. (a) The distribution of nearest distances to protons of water bound behind the selectivity filter (filled columns), averaged over a long MD simulation of closed-conductive KcsA (starting with crystal structure 1K4C), calculated for filter residues resolved in ^{1}H(^{1}H)^{13}C ssNMR experiments. The mean distances, estimated from MD simulations, are indicated. (b) Same as described in (a) for the closed-inactivated channel (starting with 1K4D). For residues V76 and T75, the nearest distances to protons of S3 water are superposed (open columns). Notably, during about 15% of the trajectory, S3 water is closer than 3.0 A to T75Hβ, which would pronounce spin diffusion transfer that exhibits a r^{-6} dependence on the internuclear distance r. (c) Snapshot of a 1K4C simulation, representative for the distribution of buried water behind the conductive filter. The ordered K$^+$ hydration shell of cavity water that was resolved in crystal structure 1K4C is illustrated below the filter. (d) Snapshot of a 1K4D simulation, representative for the distribution of buried water behind the pinched filter and the water molecule at the S3 position of the filter pore. The protons used as magnetization receptors in ^{1}H(^{1}H)^{13}C/^{15}N ssNMR experiments are highlighted with spheres. Protons for which we observed in ssNMR experiments the proximity and the absence of buried water are color-coded in yellow and green, respectively.

rate regime, on local proton−proton proximities,[19] and chemical exchange with bulk water can be neglected.[20] For ^{1}H→X transfer, we used short CP times that restrict polarization transfer to the nearest neighbor (i.e., bonded) X nucleus.[19] Thus, ^{15}N edited experiments probe proximities around NH protons, whereas ^{13}C edited experiments are sensitive to water located close to aliphatic carbons. Note that all amino protons of the selectivity filter that we use as magnetization receptors in the ^{15}N detected experiments point

directly toward the back of the filter, while aliphatic protons may be oriented toward the pore and the lower channel cavity.

First, we recorded 2D ssNMR ^{1}H(^{1}H)^{15}N spectra of membrane-embedded KcsA (see Experimental Section for a detailed description of the ssNMR setup) before and after channel inactivation. Using ^{13}C and ^{15}N resonance assignments obtained previously,[9,12,21] these data provided clear evidence for higher water occupancy behind the inactivated selectivity filter (with an open activation gate) in comparison to the
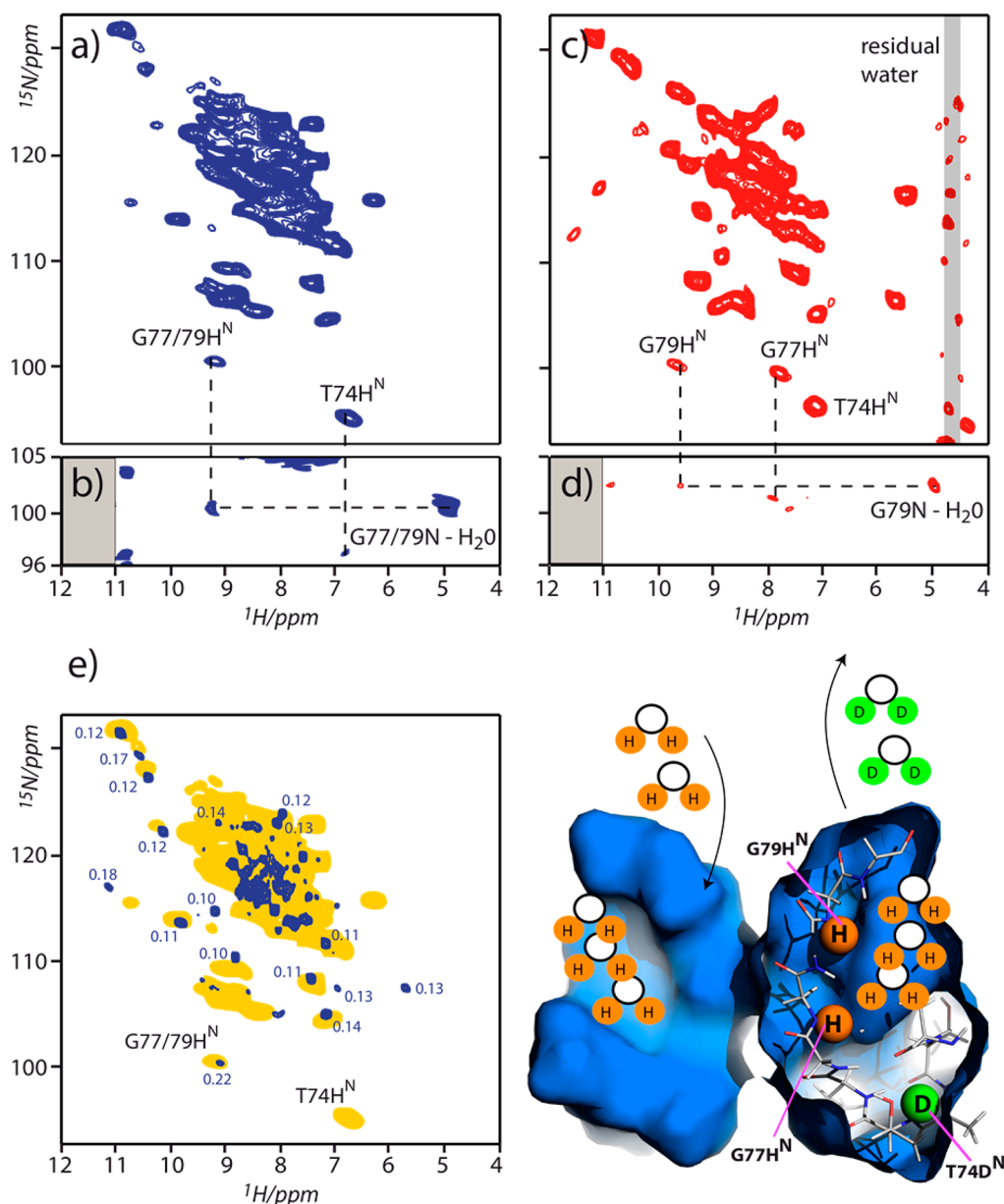
Figure 3. (a,c) 2D $^{15}N-^{1}H$ spectrum of fully protonated open-inactivated and closed-conductive KcsA, respectively, measured at 60 kHz MAS and 18.8 T static magnetic field (800 MHz ^{1}H frequency). (b,d) Cutouts of $^{1}H(^{1}H)^{15}N$ ssNMR spectra of open-inactivated and closed-conductive KcsA, respectively. The gray boxes indicate the limits of the spectral width, and the adjacent signal intensity is spurious. (e) (right) Comparison of 2D NH data on ($^{1}H,^{13}C,^{15}N$; in yellow) membrane-embedded KcsA in the open-inactivated state to an equivalent ($^{2}H,^{13}C,^{15}N$; in blue) sample after washing in acidic H_2O buffer. The blue numbers represent the ^{1}H line width at half-height (in ppm) of resolved cross-peaks and the G77/G79 signal extracted from the spectrum of the back-exchanged deuterated channel.

conductive filter conformation (with a closed activation gate). In the closed-conductive state (Figure 1a, red), only the upper part of the filter (G79N) showed an intense correlation with the water resonance, while such correlations were weak or entirely absent for residues of the middle and lower parts of the filter (T78N−T74N). In the open-inactivated state (Figure 1b, blue), buried water is distributed along the entire rear of the filter (G79−T75), with the exception of the lowest part of the filter (T74N) that is right above a large water-filled cavity. The slightly different ^{1}H shifts of water in Figure 1b may indicate the presence of several water molecules behind the inactivated filter. Taken together, these ssNMR findings for the conductive and inactivated, membrane embedded channel state are hence in excellent agreement with the spread and content of buried

water molecules in the low $[K^+]$ and high $[K^+]$ crystal structures,[13] respectively (Figure 1c).

To characterize the distribution of buried water around aliphatic protons, we carried out a 3D $^{1}H(^{1}H)^{13}C^{13}C$ experiment. For open-inactivated KcsA, this experiment (Figure 1d) revealed clear signals in the $^{13}C-^{13}C$ plane at the ^{1}H water resonance for residues Y78, V76, and T75, while T74 was absent. These findings are in line with our $^{1}H(^{1}H)^{15}N$ data (Figure 1b) and confirm that buried water is confined to the upper and the middle passages behind the inactivated filter. Interestingly, $^{13}C-^{13}C$ cross-peaks of T75, that is located close to the dewetted residue T74, were more intense than for V76. This is not inferable from the low $[K^+]$ crystal structure in which buried water is closer to V76 than to T75. The apparent

closer proximity in the inactivated filter conformation of T75 to ordered water in comparison to V76 observed by our ssNMR data could be confirmed in a series of 2D $^1H(^1H)^{13}C$ experiments with varying $^1H–^1H$ mixing time (Figure 1e–g). These results suggest that cross-peak intensities correlate to differential exposure to ordered water and that they are not modulated by the $^{13}C–^{13}C$ PARIS spin diffusion step. The same set of ^{13}C detected experiments performed on a sample in the closed-conductive state showed an exposure to ordered water that increased toward the large water-filled cavity (T75 and T74). Notably, a few protons such as T74Hβ and T75Hβ of the selectivity filter that are monitored in our ^{13}C detected experiments point toward the selectivity filter pore and the large water-filled cavity (vide infra).

These results suggested that the ^{13}C detected experiments are, in addition to water behind the selectivity filter, sensitive to the presence of other ordered water molecules. We therefore calculated the nearest distances of water to the residues that we monitor in ^{13}C detected experiments over long MD simulations for both conductive and inactivated filter conformations (Figure 2a,b). For the conductive filter, the simulations clearly showed (Figure 2a) that water behind the filter is too distant (>8.0 Å) to transfer magnetization to T75 or T74, raising the question of what causes the high water access in ^{13}C detected experiments for these two residues. Ordered water within the conductive filter pore is unlikely, because water has to transverse the filter within nanoseconds to ensure fast ion flux. We hypothesize that the increased water access stems from ordered water in the closed large cavity forming a hydration complex to help K$^+$ to overcome the high dielectric barrier of the bilayer and to position K$^+$ optimally to the filter.[13,22] Our ssNMR data suggest that both T75 and T74 are in proximity of such ordered cavity water, presumably stabilizing it with their hydroxyl functions (Figure 2c). Because the inner helix is supposed to stabilize ordered cavity water and moves outward upon channel opening, dilating the cavity,[7] water order is presumably influenced by the mode of the activation gate and therefore attenuated in the open cavity. Indeed, in the open-inactivated state, residue T74 shows weak water access in ^{13}C detected experiments (Figure 1d,g). It is interesting to think about a functional role of the close proximity of the first or second ion-hydration layer to the entrance of the selectivity filter, bearing in mind that Na$^+$ and K$^+$ feature hydration shells in the cavity that are different in shape and order and also bind there with different affinities.[13,23]

The computational analysis also confirmed that water behind the inactivated filter is closer to V76Hα than to T75Hβ (Figure 2b), which means that buried water alone is unlikely to account for the high water access of T75Hβ. Remarkably, an ordered water molecule was also cocrystallized in the inactivated filter at the S3 position.[13] Such water, as shown by simulations, is very close to T75Hβ (Figure 2b,d), often closer than 3.0 Å, and would account for its high water access in the ^{13}C detected experiments. This water in the filter featured residence times around the microsecond range in the simulations (Supporting Information Figure S1), which will be longer at the temperatures used in our ssNMR experiments (283 K).

Taken together, our ^{13}C and ^{15}N detected ssNMR data, in reference to simulations, provide a high-resolution map of the spatial distribution of ordered water around the selectivity filter. Buried water is spread all along the inactivated filter's rear with the exception of T74, and our data suggest ordered water at the S3 position in the inactivated filter (Figure 2d). In the

conductive filter, only the upper, extracellular part (G79) is in direct contact to buried water, while the rest of the filter is devoid of it. Moreover, with a closed activation gate, T75 and T74 seem to be in close proximity to the ordered hydration shell of cavity ions (Figure 2c).

High-Resolution ^1H ssNMR To Probe Water Dynamics Behind the Selectivity Filter. As an alternative and more direct means to probe the presence of buried water molecules, we resorted to high-resolution ^1H ssNMR that can be obtained by using very fast MAS rates (see, e.g., refs 24,25) and/or by perdeuteration.[26,27] In the latter case, ^1H ssNMR requires the reprotonation of protein sites via exchange with H$_2$O. For membrane proteins, this process is significantly slower for residues that are not solvent exposed and shielded by the lipid bilayer.[28] This property provided us with a unique opportunity to directly track residues that become protonated due to buried water on the time scale of channel recovery from C-type inactivation.

To ensure the identification of water-accessible and non-accessible amino-protons ($^1H^N$), we first acquired ^1H detected 2D $^{15}N–^1H$ experiments at 60 kHz MAS with fully protonated open-inactivated and closed-conductive KcsA. As compared to previous work on microcrystalline proteins,[29,30] these experiments resulted in remarkably narrow $^1H^N$ line widths of 0.3–0.5 ppm (Supporting Information Figure S2) for a membrane-embedded ion channel. Spectrally well-separated ^{15}N chemical shifts of filter residues T74, G77, and G79 allowed us to identify their $^1H^N$ both in indirectly and directly ^1H detected spectra (Figure 3a–d). To our knowledge, these assignments present the first ^1H site-specific analysis of a fully protonated membrane protein by ^1H detected biomolecular ssNMR. The resolution in our $^{15}N–^1H$ spectrum of fully protonated closed-conductive KcsA opened the possibility to monitor structural changes in reference to function in the canonical GYG motive of the K$^+$ channel superfamily. Crystal structures[13] showed G77NH to flip upon inactivation, and G77H^N indeed exhibited a stark ssNMR resonance shift ($+\Delta1.8$ ppm) to low-field in the inactivated filter conformation (Figure 3a,c). As revealed by a computational analysis, the chemical shift change of G77H^N may reflect the rotation of G77NH away from the filter's rear, where G77H^N is less exposed to the shielding ring-current effect of Y78 (Supporting Information Figure S3). Moreover, the shift of T74H^N toward high-field ($-\Delta0.5$ ppm) upon opening of the activation gate is in line with a flip of the F103 ring-plane, facing T74, which was shown to be critically involved in the coupling of activation gate and selectivity filter.[3,31] Note that such investigations of proton chemical shifts are precluded when using perdeuterated samples, because T74H^N and G77H^N are not exposed to water in all filter states (Figure 1a,b).

Next, we sought to characterize the water dynamics behind the filter by ssNMR, which is essential to convey a functional importance to buried water. Simulations demonstrated the necessity of an interchange from buried to bulk water to initiate recovery and implied long residence times for buried water to be at the molecular origin of recovery. We intended to study water dynamics by exploiting the exchangeable character of amino protons. For this purpose, we acquired 2D $^{15}N–^1H$ experiments on a membrane-embedded perdeuterated ($^2H,^{13}C,^{15}N$) KcsA sample, which was washed in an acidic (pH 3.5) H$_2$0 buffer solution. We compared our data to results obtained on the fully protonated channel, which allowed straightforward identification of $^1H^N$ of G77/G79 as water-

accessible and the $^1H^N$ of T74 as nonaccessible (Figure 3e). Importantly, protonation of G77 and G79 confirmed the presence of a pathway from bulk to buried water that is restricted to the upper part of the filter. An analysis of the ^1H line width showed that the G77/G79 $^1H^N$ signal exhibits a much larger (0.22 ppm) line width than other resolved cross-peaks (0.10−0.13 ppm), suggesting that both G77/G79 amino-deuterons exchanged to ^1H (Figure 3e). These results provide direct experimental evidence that bulk water can occupy the cavity behind the selectivity filter, as it was shown to be required for slow inactivation, and also suggest the possibility of the reverse process, release of inactivating water to the bulk, as required for recovery. Importantly, the $^1H^N$ assignments also hint at the nature of the water hydrogen-bonding network behind the inactivated selectivity filter.[22] While we observe (Figure 3e) that the $^1H^N$ of G77/G79 are water-exposed, and according to simulations[15] directly hydrogen bonded to buried water, we simultaneously observe sharp G77/G79 $^{15}N–^1H^N$ and $^{15}N–^1H^{H2O}$ correlations (Figure 3b). Hence, these experiments suggest that buried water resides behind the filter on the NMR time scale (and possibly beyond, which is in line with computational studies,[15] in which buried water remained bound behind the inactivated filter during a 17 us MD simulation).

CONCLUSIONS

Our study demonstrates the presence of several ordered water molecules surrounding the selectivity filter of membrane-embedded K$^+$ channels and that these water molecules are directly correlated with the channel gating cycle. By combining ssNMR experiments and computational data, we could sketch a high-resolution map of the spatial and temporal distribution of buried water behind the filter that clearly shows a plus of water with extended residence times behind the inactivated filter and corroborates the notion that buried water governs recovery kinetics. Moreover, we demonstrated the presence of a pathway that allows for the interchange of buried water and bulk water, as required for recovery and slow inactivation, and we find spectroscopic evidence for conformational changes of the GYG signature sequence that accompany inactivation. We want to emphasize that many of these experimental results were only possible by ^1H detection in fully protonated membrane proteins, an approach that bears the capacity to monitor protons of all protein sites irrespective of their access to water. Such studies may have far-reaching advantages to investigate exchangeable protons of the inner core of membrane and fibril proteins, which have been shown to be exceptionally stable.[28,32,33]

In general, our study illustrates the correlation between selectivity filter conformational space and the exposure to ordered water consistent with the notion of water acting as an inherent part of the gating mechanism that steers the sampling of selectivity filter conformational space. Such processes may be of general importance to the regulation of potassium channels, for instance, by heterogeneous channel opening kinetics, referred to as modal gating.[16,34] In this study, we discovered additional ordered water molecules that are located in and below the filter that could potentially act as regulatory elements of channel function. Moreover, ordered water molecules may enhance the coupling of the selectivity filter to the rest of the channel, acting as mediators that transmit conformational changes in the pore helix and turrets, which are both sensitive to the membrane environment, to the inactivation gate.[12,35]

We have demonstrated the great potential of solid-state NMR to investigate buried water molecules as an intrinsic part of ion channels in a native-like environment with the prospect of studies in native environments.[36] Such studies are of general relevance for membrane proteins, and sources of buried water as structural or functional modulators have been reported for transporters,[37] G protein coupled receptors,[38] and enzymes of the respiratory chain,[39] to name only a few examples. As it was shown by solution NMR,[40,41] such buried water molecules may be further exploited as potential probes of intrinsic protein dynamics and the underlying energy landscape.

EXPERIMENTAL SECTION

Solid-State NMR Spectroscopy. SSNMR experiments were performed using NMR spectrometers (Bruker Biospin) at magnetic fields of 16.4 and 18.8 T with 52 and 60 kHz magic angle spinning (MAS), respectively. The sample temperature was 283 K (52 kHz MAS) and 300 K (60 kHz MAS). We used 2D $^1H(^1H)^{15}N/^{13}C$ and 3D $^1H(^1H)^{13}C^{13}C$ experiments (Supporting Information Figure S4) to probe buried water molecules, transferring magnetization from rigid protons to protein heteronuclei ^{13}C or ^{15}N by a short cross-polarization step (200 us for ^{13}C, 600 us for ^{15}N). The slightly longer $^1H–^{15}N$ contact time was chosen to compensate for local backbone dynamics of the selectivity filter.[42] To facilitate transfer from buried water molecules to the protein, a short $^1H–^1H$ spin diffusion step (1.2 ms in ^{15}N and 0−2 ms in ^{13}C detected experiments) was added prior to cross-polarization. Our experimental setup is close to those used to relate membrane protein bulk water-accessibility to membrane protein conformation,[20,43,44] with the difference that a T_2 filter to suppress rigid sample components was omitted to avoid relaxation of possibly buried and rigid water molecules. Our experimental setup is sensitive to water that is immobilized on the time scale of microseconds and beyond. Note that the application of very fast MAS in this study allows the observation of ordered water molecules without the necessity of ^1H homonuclear dipolar decoupling during the ^1H evolution time. $^{13}C–^{13}C$ spin diffusion mixing at 52 kHz MAS was carried out using PARIS[17,18] with the standard pulse length = $0.5\tau_{rot}$ ($N = 0.5$) and 30 kHz recoupling amplitude over 200 ms. Heteronuclear high[45] (pulse length $0.9\tau_{rot}$) and low power[46] PISSARRO decoupling was applied during all heteronuclear and proton acquisition periods, respectively. The MISSISSPI solvent suppression scheme[47] was used in ^1H detected experiments. ^{13}C and ^{15}N resonance assignments were taken from refs 12,21.

Sample Preparation. Expression, purification, and reconstitution in asolectin of protonated uniformly ^{13}C, ^{15}N labeled KcsA followed earlier work (refs 12,48). The perdeuterated KcsA sample was expressed for 12 h to an OD600 of 1.3 in a medium containing 100% D$_2$O, uniformly ^2H, ^{13}C labeled glucose, and $^{15}NH_4Cl$. Uniformly $^2H,^{13}C,^{15}N$ labeled KcsA was washed two times for 1.5 h in 0 mM K$^+$/150 mM Na$^+$/10 mM H$_2$0 citrate buffer. Purification steps where done in neutral H$_2$0 buffers. As in refs 9,12, samples at pH 3.5 were prepared by washing proteoliposomes with 100 mM citrate buffer, yielding the same ionic strength as the phosphate buffer used for pH 7.5 samples. All reconstitution was performed at a 100/1 lipid/protein molar ratio.

Molecular Dynamics Simulations. Initial coordinates for the Molecular Dynamics simulations of the both the conductive and the pinched selectivity filters were taken from the crystal structures 1K4C and 1K4D, respectively.[13] Crystallographic water molecules for each of the four subunits of the channel were included at the start of the simulations. With the exception of Glu71, which was protonated, all residues were assigned their standard protonation state at pH 7.0. The channels were embedded in a bilayer of POPC lipids and solvated in 1.0 M KCl using the web service CHARMM-GUI (total number of atoms, 45 898). All-atom simulations were run at a temperature of 310 K under constant NVT conditions using the CHARMM PARAM27 force field. Simulations of the conductive filter were run for 510 ns, while simulations of the pinched selectivity filter were run for 17.7 μs.

All simulations were carried out on the special purpose computer Anton on loan to the Pittsburgh Supercomputer Center (PSC).[49]

ASSOCIATED CONTENT

S Supporting Information

Further details on the ssNMR experiments. Analysis of the ^{1}H detected spectra in reference to MD simulations. This material is available free of charge via the Internet at http://pubs.acs.org.

AUTHOR INFORMATION

Corresponding Authors

m.h.weingarth@uu.nl
m.baldus@uu.nl

Notes

The authors declare no competing financial interest.

ACKNOWLEDGMENTS

REFERENCES

(1) Yellen, G. *Nature* **2002**, *419*, 35−42.
(2) Doyle, D. A.; Morais Cabral, J.; Pfuetzner, R. A.; Kuo, A.; Gulbis, J. M.; Cohen, S. L.; Chait, B. T.; MacKinnon, R. *Science* **1998**, *280*, 69−77.
(3) Cuello, L. G.; Jogini, V.; Cortes, D. M.; Pan, A. C.; Gagnon, D. G.; Dalmas, O.; Cordero-Morales, J. F.; Chakrapani, S.; Roux, B.; Perozo, E. *Nature* **2010**, *466*, 272−275.
(4) Shimizu, H.; Iwamoto, M.; Konno, T.; Nihei, A.; Sasaki, Y. C.; Oiki, S. *Cell* **2008**, *132*, 67−78.
(5) Imai, S.; Osawa, M.; Takeuchi, K.; Shimada, I. *Proc. Natl. Acad. Sci. U.S.A.* **2010**, *107*, 6216−6221.
(6) Ader, C.; Schneider, R.; Hornig, S.; Velisetty, P.; Vardanyan, V.; Giller, K.; Ohmert, I.; Becker, S.; Pongs, O.; Baldus, M. *EMBO J.* **2009**, *28*, 2825−2834.
(7) Uysal, S.; Cuello, L. G.; Cortes, D. M.; Koide, S.; Kossiakoff, A. A.; Perozo, E. *Proc. Natl. Acad. Sci. U.S.A.* **2011**, *108*, 11896−11899.
(8) Cuello, L. G.; Jogini, V.; Cortes, D. M.; Perozo, E. *Nature* **2010**, *466*, 203−208.
(9) Ader, C.; Schneider, R.; Hornig, S.; Velisetty, P.; Wilson, E. M.; Lange, A.; Giller, K.; Ohmert, I.; Martin-Eauclaire, M. F.; Trauner, D.; Becker, S.; Pongs, O.; Baldus, M. *Nat. Struct. Mol. Biol.* **2008**, *15*, 605−612.
(10) Cordero-Morales, J. F.; Cuello, L. G.; Zhao, Y.; Jogini, V.; Cortes, D. M.; Roux, B.; Perozo, E. *Nat. Struct. Mol. Biol.* **2006**, *13*, 311−318.
(11) Cordero-Morales, J. F.; Cuello, L. G.; Perozo, E. *Nat. Struct. Mol. Biol.* **2006**, *13*, 319−322.
(12) van der Cruijsen, E. A.; Nand, D.; Weingarth, M.; Prokofyev, A.; Hornig, S.; Cukkemane, A. A.; Bonvin, A. M.; Becker, S.; Hulse, R. E.; Perozo, E.; Pongs, O.; Baldus, M. *Proc. Natl. Acad. Sci. U.S.A.* **2013**, *110*, 13008−13013.
(13) Zhou, Y.; Morais-Cabral, J. H.; Kaufman, A.; MacKinnon, R. *Nature* **2001**, *414*, 43−48.
(14) Domene, C.; Klein, M. L.; Branduardi, D.; Gervasio, F. L.; Parrinello, M. *J. Am. Chem. Soc.* **2008**, *130*, 9474−9480.
(15) Ostmeyer, J.; Chakrapani, S.; Pan, A. C.; Perozo, E.; Roux, B. *Nature* **2013**, *501*, 121−124.
(16) Chakrapani, S.; Cordero-Morales, J. F.; Jogini, V.; Pan, A. C.; Cortes, D. M.; Roux, B.; Perozo, E. *Nat. Struct. Mol. Biol.* **2011**, *18*, 67−74.
(17) Weingarth, M.; Demco, D. E.; Bodenhausen, G.; Tekely, P. *Chem. Phys. Lett.* **2009**, *469*, 342−348.
(18) Weingarth, M.; Bodenhausen, G.; Tekely, P. *J. Am. Chem. Soc.* **2009**, *131*, 13937−13939.
(19) Lange, A.; Seidel, K.; Verdier, L.; Luca, S.; Baldus, M. *J. Am. Chem. Soc.* **2003**, *125*, 12640−12648.
(20) Ader, C.; Schneider, R.; Seidel, K.; Etzkorn, M.; Becker, S.; Baldus, M. *J. Am. Chem. Soc.* **2009**, *131*, 170−176.
(21) Schneider, R.; Ader, C.; Lange, A.; Giller, K.; Hornig, S.; Pongs, O.; Becker, S.; Baldus, M. *J. Am. Chem. Soc.* **2008**, *130*, 7427−7435.
(22) Roux, B.; MacKinnon, R. *Science* **1999**, *285*, 100−102.
(23) Zhou, Y.; MacKinnon, R. *Biochemistry* **2004**, *43*, 4978−4982.
(24) Parthasarathy, S.; Nishiyama, Y.; Ishii, Y. *Acc. Chem. Res.* **2013**, *46*, 2127−2135.
(25) Zhou, D. H.; Rienstra, C. M. *Angew. Chem., Int. Ed.* **2008**, *47*, 7328−7331.
(26) McDermott, A. E.; Creuzet, F. J.; Kolbert, A. C.; Griffin, R. G. *J. Magn. Reson.* **1992**, *98*, 408−413.
(27) Chevelkov, V.; Rehbein, K.; Diehl, A.; Reif, B. *Angew. Chem., Int. Ed.* **2006**, *45*, 3878−3881.
(28) Shi, L.; Kawamura, I.; Jung, K. H.; Brown, L. S.; Ladizhansky, V. *Angew. Chem., Int. Ed.* **2011**, *50*, 1302−1305.
(29) Zhou, D. H.; Nieuwkoop, A. J.; Berthold, D. A.; Comellas, G.; Sperling, L. J.; Tang, M.; Shah, G. J.; Brea, E. J.; Lemkau, L. R.; Rienstra, C. M. *J. Biomol. NMR* **2012**, *54*, 291−305.
(30) Marchetti, A.; Jehle, S.; Felletti, M.; Knight, M. J.; Wang, Y.; Xu, Z. Q.; Park, A. Y.; Otting, G.; Lesage, A.; Emsley, L.; Dixon, N. E.; Pintacuda, G. *Angew. Chem., Int. Ed.* **2012**, *51*, 10756−10759.
(31) Pan, A. C.; Cuello, L. G.; Perozo, E.; Roux, B. *J. Gen. Physiol.* **2011**, *138*, 571−580.
(32) Ritter, C.; Maddelein, M. L.; Siemer, A. B.; Luhrs, T.; Ernst, M.; Meier, B. H.; Saupe, S. J.; Riek, R. *Nature* **2005**, *435*, 844−848.
(33) Van Melckebeke, H.; Schanda, P.; Gath, J.; Wasmer, C.; Verel, R.; Lange, A.; Meier, B. H.; Bockmann, A. *J. Mol. Biol.* **2011**, *405*, 765−772.
(34) Popescu, G. K. *J. Physiol.* **2012**, *590*, 73−91.
(35) Weingarth, M.; Prokofyev, A.; van der Cruijsen, E. A.; Nand, D.; Bonvin, A. M.; Pongs, O.; Baldus, M. *J. Am. Chem. Soc.* **2013**, *135*, 3983−39888.
(36) Renault, M.; Tommassen-van Boxtel, R.; Bos, M. P.; Post, J. A.; Tommassen, J.; Baldus, M. *Proc. Natl. Acad. Sci. U.S.A.* **2012**, *109*, 4863−4868.
(37) Hung, L. W.; Wang, I. X.; Nikaido, K.; Liu, P. Q.; Ames, G. F.; Kim, S. H. *Nature* **1998**, *396*, 703−707.
(38) Angel, T. E.; Chance, M. R.; Palczewski, K. *Proc. Natl. Acad. Sci. U.S.A.* **2009**, *106*, 8555−8560.
(39) Schmidt, B.; McCracken, J.; Ferguson-Miller, S. *Proc. Natl. Acad. Sci. U.S.A.* **2003**, *100*, 15539−15542.
(40) Denisov, V. P.; Peters, J.; Horlein, H. D.; Halle, B. *Nat. Struct. Biol.* **1996**, *3*, 505−509.
(41) Persson, F.; Halle, B. *J. Am. Chem. Soc.* **2013**, *135*, 8735−8748.
(42) Ader, C.; Pongs, O.; Becker, S.; Baldus, M. *Biochim. Biophys. Acta* **2009**, *1798*, 286−290.
(43) Luo, W.; Hong, M. *J. Am. Chem. Soc.* **2010**, *132*, 2378−2384.
(44) Kumashiro, K. K.; Schmidt-Rohr, K.; Murphy, O. J.; Ouellette, K. L.; Cramer, W. A.; Thompson, L. K. *J. Am. Chem. Soc.* **1998**, *120*, 5043−5051.
(45) Weingarth, M.; Tekely, P.; Bodenhausen, G. *Chem. Phys. Lett.* **2008**, *466*, 247−251.
(46) Weingarth, M.; Bodenhausen, G.; Tekely, P. *J. Magn. Reson.* **2009**, *199*, 238−241.
(47) Zhou, D. H.; Rienstra, C. M. *J. Magn. Reson.* **2008**, *192*, 167−172.

(48) Lange, A.; Giller, K.; Hornig, S.; Martin-Eauclaire, M. F.; Pongs, O.; Becker, S.; Baldus, M. *Nature* **2006**, *440*, 959−962.

(49) Shaw, D. E.; Dror, O. R.; Salmon, J. K.; Grossman, J. P.; Mackenzir, K. M.; Bank, J. A.; Young, C.; Deneroff, M. M.; Batson, B.; Bowers, E. C.; Eastwood, M. P.; Ierardi, D. J.; Klepeis, J. L.; Kuskin, J. S.; Larson, R. H.; Lindorff-Larsen, K.; Maragakis, P.; Moraes, M. A.; Piana, S.; Shan, Y.; Towles, B. *Proc. Conf. High Performance Computing Networking, Storage Anal.* **2009**, 1−11.